https://doi.org/10.5194/hess-2020-1
Preprint. Discussion started: 16 January 2020

Hydrology and Earth System Sciences
Discussions
Open Access

Novel Keeling plot based methods to estimate the isotopic composition of ambient water vapor

Yusen Yuan[a,b], Taisheng Du[a]*, Honglang Wang[c], Lixin Wang[b]*

[a] Center for Agricultural Water Research in China, China Agricultural University, Beijing 100083, China
[b] Department of Earth Sciences, Indiana University-Purdue University Indianapolis, Indianapolis, Indiana 46202, USA
[c] Department of Mathematical Sciences, Indiana University-Purdue University Indianapolis, Indianapolis, Indiana 46202, USA

* Corresponding author: Dr. Taisheng Du
Fax: +86-10-62737611; Tel: +86-10-62738398
Email: dutaisheng@cau.edu.cn

* Corresponding author: Dr. Lixin Wang
Fax: +1-1-317-274-7966; Tel: +1-317-274-7764
Email: lxwang@iupui.edu

Highlights:

1. Two new methods were developed to estimate the isotopic composition of ambient vapor.
2. Theoretical derivations were provided for these two methods.
3. Linear regression showed strong agreement between the two methods.
4. The methods provide a possibility to calculate the proportion of evapotranspiration fluxes to total atmospheric vapor using the same instrumental setup for the traditional Keeling plot investigations.

https://doi.org/10.5194/hess-2020-1
Preprint. Discussion started: 16 January 2020

Abstract

Keeling plot approach, a general method to identify the isotopic composition of source atmospheric CO_2 and water vapor (i.e., evapotranspiration), has been widely used in terrestrial ecosystems. The isotopic composition of ambient water vapor (δ_a), another important source of atmospheric water vapor, is not able to be estimated to date using the Keeling plot approach. Here we proposed two new methods to estimate δ_a using the Keeling plot curves: one using intersection point method and another replying on intermediate value theorem. As actual δ_a value was difficult to measure directly, we used two indirect approaches to validate our new methods. First, we made an external vapor tracking using Hybrid Single Particle Lagrangian Integrated Trajectory (HYSPLIT) model to facilitate explaining the variation of δ_a. The trajectory vapor origin results were consistent with the expectations of the δ_a values estimated by these two methods. Second, regression analysis was used to evaluate the relationship between δ_a values estimated from these two independent methods and they are in strong agreement. This study provides an analytical framework to estimate δ_a using existing facilities, and provides important insights into the traditional Keeling plot approach by showing: (a) an evidence that δ_a was constant in a certain moment among different heights, a key assumption of the Keeling plot approach, (b) a possibility to calculate the proportion of evapotranspiration fluxes to total atmospheric vapor using the same instrumental setup for the traditional Keeling plot investigations, and c) perspectives on estimation of isotope composition of ambient CO_2 ($\delta_a{}^{13}C$).

Key words: HYSPLIT, intersection point, Intermediate Value Theorem, Keeling plot

https://doi.org/10.5194/hess-2020-1
Preprint. Discussion started: 16 January 2020

1. Introduction

Stable isotopes of hydrogen and oxygen ($^1H^2HO$ and $H_2{}^{18}O$) have been widely used in root water uptake source identification (Corneo et al., 2018; Mahindawansha et al., 2018) and evapotranspiration (ET) partitioning (Brunel et al., 1997) in terrestrial ecosystems based on Craig-Gordon model (Craig and Gordon, 1965), isotope mass balance and mechanism of isotopic fractionation (Majoube, 1971; Merlivat and Jouzel, 1979). After laser spectrometers being utilized to perform continuous high frequency (1 Hz) measurements of the isotopic composition of atmospheric water vapor (δ_v) and atmospheric water vapor content (C_v) (Kerstel and Gianfrani, 2008; Wang et al., 2009), new insights into processes that affect δ_v and the number of studies based on continuous ground level isotope measurements was continuously increasing (Wang et al., 2010; Galewsky et al., 2011; Steen-Larsen et al., 2013; Sprenger et al., 2015). Such increase in isotope data abundance allows an isotope-enabled global circulation models (Iso-GCMs) to estimate the variation of vapor isotope parameters at a global scale (Unger et al., 2010).

Keeling plot approach (Keeling, 1958), based on isotope mass balance and two-source assumption, was first used to explain carbon isotope ratios of atmosphere CO_2 and to identify the sources that contribute to increases in atmospheric CO_2 concentration. It has been further used to estimate isotopic composition of ET (δ_{ET}) in recent two decades (Yakir and Sternberg, 2000). Keeling plot analyses can be applied using δ_v and C_v output by laser based analyzer either from different heights (Yepez et al., 2003; Zhang et al., 2011; Good et al., 2012) or at one height with continuous observations (Wei et al., 2015; Keppler et al., 2016). Although the intercept of the curve was commonly used, the slope of the Keeling plot was also used to

https://doi.org/10.5194/hess-2020-1
Preprint. Discussion started: 16 January 2020

estimate δ_{ET} by re-arranging the Keeling plot equations (Miller and Tans, 2003; Fiorella et al., 2018). Keeling plot approach was based on bulk water and isotope mass balance using two equations with three unknowns. As a result, the isotopic composition of other potential sources (e.g., water vapor not from ET), as well as isotopic composition of ambient water vapor (δ_a), were not able to be estimated directly using the Keeling plot approach.

In this study, we proposed two new methods to estimate δ_a, one based on the intersection of two Keeling plots of two continuous observation moments and another based on intermediate value theorem. Proposition and proof were provided, and the new methods were tested using field observations. As direct observations of δ_a rarely exist (Griffis et al., 2016), we tested our methods by (a) making an external water vapor tracking investigation according to HYSPLIT model to explain the variation of estimated δ_a, and (b) making a regression analysis using δ_a estimated by these two independent methods.

2. Materials and Methods

2.1 Theory

The atmospheric vapor concentration in an ecosystem reflects the combination of ambient vapor that is already exist in the atmosphere and the vapor that is added through evaporation (E) and transpiration (T) (Yakir and Sternberg, 2000). Keeling plot approach is based on the combination of a bulk water mass balance equation and an isotope mass balance equation:

$$C_v = C_a + C_{ET} \quad , \quad (1)$$

$$C_v\delta_v = C_a\delta_a + C_{ET}\delta_{ET} \quad , \quad (2)$$

where δ_a, δ_{ET} and δ_v are isotope composition of ambient water vapor, ET, and atmospheric water vapor, respectively, and C_a, C_{ET} and C_v are the corresponding concentrations of water vapor. Note that all quantities here are time dependent, and δ_v and C_v also depend on heights.

Combining Eq. (1) and Eq. (2), we have the following traditional linear Keeling plot relationship between δ_v and $1/C_v$ with intercept δ_{ET} and slope $C_a(\delta_a - \delta_{ET})$,

$$\delta_v = C_a(\delta_a - \delta_{ET})/C_v + \delta_{ET} \quad . \tag{3}$$

For a given time, with various measurements of δ_v and C_v collected at different heights, we are able to estimate the intercept δ_{ET} and slope $C_a(\delta_a - \delta_{ET})$ for this moment from regression analysis (Zhang et al., 2011; Wang et al., 2013). Here we focus on the estimation of δ_a using two new methods proposed below.

Intersection point method. Note that for two nearby time points t_1 and t_2, we could use local constant approximation to estimate δ_a within this time interval since it is changing smoothly over time. By assuming local constant for C_a and δ_a within this time interval, we have

$$\delta_{v_1} = C_a(\delta_a - \delta_{ET_1})/C_{v_1} + \delta_{ET_1} \quad , \tag{4}$$

$$\delta_{v_2} = C_a(\delta_a - \delta_{ET_2})/C_{v_2} + \delta_{ET_2} \quad , \tag{5}$$

where δ_{ET_i}, δ_{v_i} and C_{v_i} represent the value at t_i for i=1, 2. From (4) and (5), we can solve δ_a as:

$$\delta_a = \frac{C_{v_1}\delta_{ET_2}(\delta_{ET_1}-\delta_{v_1}) - C_{v_2}\delta_{ET_1}(\delta_{ET_2}-\delta_{v_2})}{C_{v_1}(\delta_{ET_1}-\delta_{v_1}) - C_{v_2}(\delta_{ET_2}-\delta_{v_2})} \quad . \tag{6}$$

The local constant approximation idea was first described in Yamanaka and Shimizu (2007) as an assumption to quantify the contribution of local ET to total atmospheric vapor.

Intermediate Value Theorem (IVT) method. Denote the slope as $k = C_a(\delta_a - \delta_{ET})$. Since $C_a < C_v = C_a + C_{ET}$, we have $C_a = \frac{k}{(\delta_a - \delta_{ET})} < C_v$. We can rearrange $\frac{k}{(\delta_a - \delta_{ET})} < C_v$ to attain δ_a: $\delta_a < \frac{k}{C_v} + \delta_{ET} = \delta_v$ when $k < 0$, and $\delta_a > \frac{k}{C_v} + \delta_{ET} = \delta_v$ when $k > 0$.

For the smooth function $\delta_{\mathrm{a}}(t)$ defined on the interval $[t_1, t_2]$ with the two time points satisfying $k(t_1)\,k(t_2) < 0$, depending on the sign of the slopes $k(t_1)$ and $k(t_2)$ and the order of $\delta_{v_1} = \delta_{\mathrm{v}}(t_1)$ and $\delta_{v_2} = \delta_{\mathrm{v}}(t_2)$ at the two time points t_1 and t_2, it will correspond to one of the six cases in **Fig. 1**. For all of the six situations, by the intermediate value theorem, there exists a sub-interval $[t_1{}', t_2{}'] \subset [t_1, t_2]$ such that the whole range of $\{\delta_{\mathrm{a}}(t): t \in [t_1', t_2']\}$ is within $[min(\delta_{v_1}, \delta_{v_2}), max(\delta_{v_1}, \delta_{v_2})]$. Thus for the two nearby time points t_1 and t_2 with k_1 and k_2 having different sign, δ_a will be between δ_{v_1} and δ_{v_2}. This is the key observation to estimate the parameter of interest δ_a based on Intermediate Value Theorem, which leads to approximation of δ_a within the time interval between t_1 and t_2 using δ_{v_1} and δ_{v_2}:

$$\delta_a \approx \frac{\delta_{v_1} + \delta_{v_2}}{2} \qquad . \qquad (7)$$

Using this method, we are able to compute δ_a using data points when the slopes of Keeling plots change sign between two adjacent time points.

2.2 Field observations

2.2.1 Study site

A field measurement was conducted over a maize field (39 ha) from 1st May 2017 to 1st September 2017 at Shiyanghe Experimental Station of China Agricultural University, located in Wuwei of Gansu Province, northwest China (37°85′N, 102°88′E; altitude 1581m). The region belongs to temperate continental climate and is in the oasis within the Shiyang river basin. The annual mean temperature of the study area is about 8.8℃ with pan evaporation of 2000 mm, annual precipitation of 164.4 mm, mean sunshine duration of 3000 h, and frost-free period of more than 150 d. The local crops are irrigated using groundwater with electrical conductivity of 0.62 dSm^{-1}. The groundwater table is 30-40 m below the surface. Maize was

https://doi.org/10.5194/hess-2020-1
Preprint. Discussion started: 16 January 2020

sowed on 23 April and harvested on 15 September 2017, with row spacing of 40 cm and plant spacing of 23 cm. The maize growing stage was divided into seedling stage (April 21st –May 20th), jointing stage (May 21st-July 10th), heading period (July 11th-July 31st), pustulation period (August 1st-August 31st) and mature period (September 1st-September 20th).

2.2.2 Instrument setup and measurement design

A 24-meter flux tower, located in the middle of maize field, was used to measure ET flux and isotopic composition of water vapor at different heights. The field is approximately 600 m long and 240 m wide, with a 10% slope decreasing from southwest to northeast. Five gas traps were installed on the flux tower at heights of 4 m, 8 m, 12 m, 16 m and 20 m, respectively. An iron pillar was placed 20 m away from the flux tower. Three gas traps were installed on the iron pillar, one was close to the canopy, and the other two were 2 m and 3 m above the ground. Canopy gas trap was adjusted weekly according to the height of maize.

In situ δ_v and C_v collected by the eight gas traps were monitored by an isotope and gas concentration analyzer (L2130-i, Picarro Inc., Sunnyvale, CA, USA), which was a wavelength scanned cavity ring down spectroscope (WS-CRDS) instrument. Vapor specifications include a measurement range from 1000 to 50000 ppm, the precision is 0.040‰ to 0.25‰ for $\delta^{18}O$ (Zhao et al., 2019). Interfacing with the gas trap and the isotope analyzer, Teflon tube was wrapped by thermal insulation cotton to avoid vapor condensation during transmission. The measurement of δ_v and C_v on 19th May, 11th June, 20th July, and 12th August were selected to test the theoretical framework because they fit the criteria requirements of the IP method and IVT method: 1) a complete and continuous 24-hour dataset and 2) opposite Keeling plots slope occurrence at least once in a day. These four days corresponded to seedling stage, jointing stage,

https://doi.org/10.5194/hess-2020-1
Preprint. Discussion started: 16 January 2020

heading stage, and pustulation stage, respectively, through the maize growth period.

2.2.3 Calibration of δ_v and C_v

The water vapor from eight inlets were sampled continuously over a 24-hour-period. Since only one analyzer was used to measure the δ_v and C_v, the values of eight sampling inlets were recorded in turn every 225s in a 30 mins cycle. The switch procedure was automatic. As the analyzer makes a measurement every 0.9-1s, approximately 259-264 values for each inlet was recorded within the cycle. For each 225s measurement period, No. 195 to No. 253 data points were used to avoid memory issue and influence of transient pressure variation. The mean value of the selected data points was regarded as the measured δ_v and C_v in a specific inlet. Measured C_v was used directly as actual C_v, while measured δ_v was calibrated to minimize the influence of isotopic concentration dependence. The C_v in our measurement ranged from 5386 ppm to 30255 ppm. Thus, C_v gradients of 10000 ppm, 20000 ppm and 30000 ppm were selected as calibration concentrations to improve the precision of δ_v.

2.3 Explanations of δ_a using backward trajectories

To explain the variations of estimated δ_a, air mass backward trajectories were calculated using the Hybrid Single Particle Lagrangian Integrated Trajectory (HYSPLIT) model (Draxler and Hess, 1997; Draxler, 2003; Stein et al., 2015; Kaseke et al., 2018) and meteorological data from the Global Data Assimilation System 0.5 Degree (GDAS0p5) with 0.5°×0.5° spatial resolution and 3-hour time resolution for the selected four days. Five hundred meters height was selected in the modeling. Each backward trajectory was initialized from the station (37°85′N, 102°88′E) at 12:00 pm (local time), and calculated backward for 72 hours. Four trajectories were computed.

https://doi.org/10.5194/hess-2020-1
Preprint. Discussion started: 16 January 2020

3. Results

3.1 Diurnal variations of δ_{ET}, δ_v, k and ambient vapor source in four typical days during the maize growing period

The parameters of the Keeling plot curve in four typical days were shown in **Fig. 2**. The average δ_{ET} were -15.23‰, -10.20‰, -8.20‰ and -10.59‰, respectively in the four typical days. At daytime (7:00am-7:00pm), average δ_{ET} were -11.75‰, -8.42‰, -5.76‰ and -9.00‰, respectively, while at nighttime (7:00pm-7:00am the next day), average δ_{ET} were -18.76‰, -11.98‰, -10.63‰ and -12.18‰, respectively. The trend of δ_v values were similar to δ_{ET}, but with a smaller fluctuation than δ_{ET}. About 65% of k values were negative during the four days, and most positive k values occurred at nighttime (82%). The 500 m height water vapor backward trajectories revealed that vapor was from outside the study regions on 19th May and 20th July while vapor was from local ET on 11th June and 12th August **(Fig. 3)**.

3.2 Diurnal variations of δ_a using two methods during the maize growing period

Data screening was needed on the calculation of δ_a. When δ_a was not satisfied with the relationship of $\delta_{ET}<\delta_v<\delta_a$ or $\delta_{ET}>\delta_v>\delta_a$, these δ_a values were in contradiction with Eq. (1) and were not used. As a result, 88 and 26 of δ_a values were attained based on IP method and IVT method, respectively during the four days **(Fig. 2)**.

As for the IP method, 46.8% of δ_a values were acceptable, and 59.1% of acceptable δ_a values were during the daytime (7:00am-7:00pm). The average δ_a values were -12.95‰, -12.13‰, -14.39‰ and -12.77‰ for the four days, respectively. Smaller values occurred on 19th May (-12.95‰) and 20th July (-14.39‰) than those on 11^{h} June (-12.13‰) and 12th August (-12.77‰). The average δ_a values in all four days were -13.60‰ and -12.04‰ during the

https://doi.org/10.5194/hess-2020-1
Preprint. Discussion started: 16 January 2020

daytime and the nighttime, respectively.

As for the IVT method, only 13.8% of δ_a values were acceptable, and 34.6% of acceptable δ_a values were during the daytime (7:00am-7:00pm). The average δ_a values were -13.93‰, -11.03‰, -14.76‰ and -11.83‰ for the four days, respectively. Smaller values occurred on 19th May (-13.93‰) and 20th July (-14.67‰) than those on 11th June (-11.03‰) and 12th August (-11.83‰). The average δ_a values in all four days were -12.84‰ and -12.86‰ during the daytime and the nighttime, respectively.

Fourteen observation periods overlapped for δ_a calculation using both methods, which accounted for 15.9% of δ_a values using IP method ($\delta_{a(IP)}$) and 53.8% of δ_a values using IVT method ($\delta_{a(IVT)}$). Linear regression between $\delta_{a(IP)}$ and $\delta_{a(IVT)}$ was significant for these fourteen observation periods with slope close to one (**Fig. 4**. $\delta_{a(IP)} = 0.95\delta_{a(IVT)} - 0.75$, $R^2 = 0.98$, $p<0.01$, $n=14$).

4. Discussion

4.1 The reliability of δ_a estimating methods

The IP method was based on the assumption that the ambient sources were the same between two continuous observation moments. This is a reasonable assumption for short time intervals. For the IVT method, δ_a was derived from δ_v in two continuous moments when their Keeling plot slopes were opposite. The opposite slopes of the Keeling plots were the only requirement. As δ_v was almost constant in two continuously moments, $\delta_{a(IVT)}$ was able to be constrained into a small range. The derivation was supported by the intermediate value theorem. Therefore, both methods of estimating δ_a were theoretically sound.

The δ_a results were also examined by HYSPLIT backward trajectories to identify the

https://doi.org/10.5194/hess-2020-1
Preprint. Discussion started: 16 January 2020

Hydrology and Earth System Sciences
Open Access
Discussions

different sources of water vapor, which assesses the reliability of both methods indirectly. Based on the trajectory analysis, water vapor in the study area came from westerlies, northern polar region and local recirculation. Water vapor from southwest monsoon and northwest Pacific were not detected in this study. Based on the isotope variation of meteoric water (Fricke et al., 1999), water vapor from westerlies and northern polar was more ^{18}O depleted than local recycled moisture through ET. It was also reported that the water vapor from outside the study regions will lower δ_v values (Ma et al., 2014; Chen et al., 2015). Backward trajectory revealed the local origin of water vapor on 11th June and 12th August. The calculated δ_a values on 11th June and 12th August based on the IP method and interval intermediate value theorem approach was higher than those in other two days, which was consistent with our expectation. The results indicate that quantifying δ_a using the IP method and intermediate value theorem approach was reliable. The reliability of two methods were also supported by the close relationship of δ_a using these two independent methods.

4.2 The application of δ_a for moisture recycling

When δ_a was estimated, moisture recycling (e.g., f_{ET}, the contribution of ET fluxes to the total water vapor) can be estimated using the following equations with known δ_a, δ_{ET}, δ_v, C_{ET} and C_v:

$$C_{ET} = C_v \bullet \frac{\delta_a - \delta_v}{\delta_a - \delta_{ET}} \quad , \qquad (8)$$

$$f_{ET} = \frac{C_{ET}}{C_v} \quad , \qquad (9)$$

According to Eq. (8) and Eq. (9), f_{ET} was only related to δ_a, δ_V, and δ_{ET}. These three parameters were obtained for relatively small temporal and spatial scales in this study, making it possible to estimate f_{ET} at a tower scale. The f_{ET} estimate will provide a baseline value for

https://doi.org/10.5194/hess-2020-1
Preprint. Discussion started: 16 January 2020

rainfall recycling ratio calculations. Previous studies quantified the contribution of recycled vapor to annul or monthly precipitation in river basins using two-element mixture model (Kong et al., 2013) and three-element mixture (Peng et al., 2011). At the watershed scale, recycled vapor rate refers to the contributions of moisture from terrestrial ET to annul or monthly precipitation (Trenberth, 1999). It is a key part of local water cycle and the atmospheric water vapor balance (Seneviratne et al., 2006; Aemisegger et al., 2014). In our study, the role of f_{ET} to regional vapor is similar to the role of recycled vapor rate to annul or monthly precipitation, but f_{ET} was calculated with fine temporal (e.g., hourly) and spatial (i.e., field scale) scales. At the watershed scale, assumption was made that no isotopic fractionation between transpiration and source water (Flanagan et al., 1991); advected vapor was assumed to be the precipitation vapor of the upwind station (Peng et al., 2011). However, the isotope composition of transpiration is variable in a day especially under non-steady-state conditions (Farquhar and Cernusak, 2005; Lai et al., 2008). In addition, sometimes it is difficult to select an upwind station without precipitation events. In this study, a field site was selected to calculate the proportion of ET fluxes to total atmospheric vapor and f_{ET} was only related to δ_a, δ_V, and δ_{ET} according to Eq. (8) and Eq. (9). This indicates that f_{ET} calculations is possible for small temporal and spatial scales after estimating δ_a using the methods we proposed.

4.3 Implications of δ_a

The signature of δ_E and δ_T was first introduced by a hypothetical graph shown on **Fig. 5a** (Moreira et al., 1997). Line 1 and line 2 was idealized Keeling plot with pure T and pure E, and Line 3 was the Keeling plot with mixed T and E. The IVT method in this study provided a general explanation of this figure. As T is a major component of ET in the daytime in non-arid

https://doi.org/10.5194/hess-2020-1
Preprint. Discussion started: 16 January 2020

region, the slope is generally negative. When E dominates ET in an ecosystem, such as in the nighttime in non-arid region or in arid region, the slope should be positive. Mathematically, negative slope is due to $\delta_{ET} < \delta_a$ and positive slope is due to $\delta_{ET} > \delta_a$. It also reflected that IVT method could only be used in non-arid ecosystems. Yamanaka and Shimizu (2007) used the assumption that δ_a of an area of 219.9 km^2 was represented by the intersection point of two Keeling plot lines in different sites with synchronous measurements and they used the intersection value as an approximate value of δ_a. This study was conducted in a maize field using 30-min interval measurements, the results indicate that accurate $\delta_{a(IP)}$ could be estimated from the intersection of two Keeling plots regardless the slope being positive or negative, while the $\delta_{a(IVT)}$ should be restricted in the area between two dotted lines as shown in **Fig. 5b** (i.e., between the minimum value of δ_v in positive slope and the maximum value of δ_v in negative slope).

While this study is about water vapor ^{18}O, the "Keeling plot" was first used by Keeling (1958, 1961) to interpret carbon isotope ratios of mixed CO_2 and to identify the sources that contribute to increases in atmospheric CO_2 concentrations on a regional basis. Compared with ET in water vapor which is consisted of E and T, net ecosystem CO_2 exchange (NEE) is comprised of soil respiration (R) and gross primary productivity (GPP). As $^{13}CO_2$ isotopic Keeling plot reveals a positive slope during both daytime and nighttime (Yakir and Wang, 1996; Unger et al., 2010), the IVT method may not be able to estimate ambient $^{13}CO_2$ isotopic composition ($\delta_a{}^{13}C$) since there are no opposite slopes in a day. In such case, the IP method may be implemented in two continuous moments to estimate $\delta_a{}^{13}C$ and may consequently further calculate the contribution of NEE to atmospheric CO_2.

https://doi.org/10.5194/hess-2020-1
Preprint. Discussion started: 16 January 2020

5. Conclusions

In this study, we established two methods to quantify δ_a using intersection point method and the Intermediate Value Theorem method. The IVT method was used under the condition of opposite slope of Keeling plots in two continuously moments. The results of estimated $\delta_{a(IP)}$ and $\delta_{a(IVT)}$ were consistent with the expectation whether it was local origin or regional origin using external vapor tracking investigation by HYSPLIT model. The linear regression between $\delta_{a(IP)}$ and $\delta_{a(IVT)}$ was highly (R^2=0.98, $p < 0.01$) significant.

This study provided insights into the traditional Keeling plot and provided two methods to estimate δ_a using the same instrumental setup for the traditional Keeling plot investigations. The results shown an evidence that δ_a was constant in a certain moment among different heights, a key assumption of Keeling plot approach. The estimated δ_a will make it possible to calculate the ET contribution to regional vapor at a 30 min interval at field scale. The results indicate that using similar framework, $\delta_a{}^{13}C$ is also solvable by the IP method.

6. Acknowledgements

We acknowledge support from the National Natural Science Foundation of China (51725904, 51621061, 51861125103), the National Key Research Program (2016YFC0400207), the Discipline Innovative Engineering Plan (111 Program, B14002) and the Division of Earth Sciences of National Science Foundation (EAR-1554894). We thank Dr. Qianning Liu from Jiangxi University of Finance and Economics and Dr. Zhengxiang Chen from Capital Normal University for checking the validity of the Intermediate Value Theorem method.

7. Code and Data availability

Code and data are available on request.

8. Author contribution

YY, TD and LW conceptualized the main research questions. YY collected data and performed the data analyses. YY and LW wrote the first draft. HW contributed to additional data analyses. All the authors contributed ideas and edited the manuscript.

9. Competing interests

There authors declare no competing interests.

10. References

Aemisegger, F., Pfahl, S., Sodemann, H., Lehner, I., Seneviratne, S. I., and Wernli, H.: Deuterium excess as a proxy for continental moisture recycling and plant transpiration, **Atmospheric Chemistry and Physics**, 14, 4029–4054, doi: 10.5194/acp-144029-2014, 2014.

Brunel, J. P., Walker, G. R., Dighton, J. C., and Monteny, B.: Use of stable isotopes of water to determine the origin of water used by the vegetation and to partition evapotranspiration. A case study from HAPEX-Sahel, **Journal of Hydrology**, 188–189, 466–481, doi:10.1016/s0022-1694(96)03188-5, 1997.

Chen, F. L., Zhang, M. J., Ma, Q., Wang, S. J., Li, X. F., and Zhu, X. F.: Stable isotopic characteristics of precipitation in Lanzhou city and its surrounding areas, Northwest China, **Environmental Earth Sciences**, 73, 4671–4680, doi: 10.1007/s12665-014-3776-6, 2015.

Corneo, P. E., Kertesz, M. A., Bakhshandeh, S., Tahaei, H., Barbour, M. M., and Dijkstra, F. A.: Studying root water uptake of wheat genotypes in different soils using water $\delta^{18}O$ stable isotopes, **Agriculture, Ecosystems & Environment**, 264, 119-129, doi: 10.1016/j.agee.2018.05.007, 2018.

Craig, H. and Gordon, L. I.: Deuterium and oxygen 18 variations in the ocean and marine atmosphere, in: **Stable Isotopes in Oceanographic Studies and Paleotemperatures**, p. 9, 1965.

Draxler, R. R., and Hess, G.: Description of the HYSPLIT4 modeling system, **NOAA Tech Memo ERL ARL-224**, Dec, 24p., 1997.

Draxler, R. R.: Evaluation of an ensemble dispersion calculation, **Journal of Applied Meteorology**, 42, 308-317, doi: 10.1175/1520-0450(2003)042<0308:EOAEDC>2.0.CO;2, 2003.

Farquhar, G. D., and Cernusak, L. A.: On the isotopic composition of leaf water in the non-steady state, **Functional Plant Biology**, 32(4), 293-303, doi: 10.1071/FP04232, 2005.

Fiorella, R. P., Poulsen, C. J., and Matheny, A. M.: Seasonal patterns of water cycling in a deep, continental mountain valley inferred from stable water vapor isotopes, **Journal of Geophysical Research: Atmospheres**, 123, 7271-7291, doi: 10.1029/2017JD028093, 2018.

Flanagan, L. B., Comstock, J. P., and Ehleringer, J. R.: Comparison of modeled and observed

https://doi.org/10.5194/hess-2020-1
Preprint. Discussion started: 16 January 2020

environmental influences on the stable oxygen and hydrogen isotope composition of leaf water in Phaseolus vulgaris L, **Plant Physiology**, 96, 588-596, doi: https://doi.org/10.1104/pp.96.2.588, 1991.

Fricke, H. C., O'Neil, J. R. J. E., and Letters, P. S.: The correlation between $^{18}O/^{16}O$ ratios of meteoric water and surface temperature: its use in investigating terrestrial climate change over geologic time, **Earth and Planetary Science Letters**, 170, 181-196, doi: 10.1016/S0012-821X(99)00105-3, 1999.

Galewsky, J., Rella, C., Sharp, Z., Samuels, K., and Ward, D.: Surface measurements of upper tropospheric water vapor isotopic composition on the Chajnantor Plateau, Chile, **Geophysical Research Letters**, 38, 1-5, doi: 10.1029/2011GL048557, 2011.

Good, S. P., Soderberg, K., Wang, L., and Caylor, K. K.: Uncertainties in the assessment of the isotopic composition of surface fluxes: A direct comparison of techniques using laser-based water vapor isotope analyzers, **Journal of Geophysical Research: Atmospheres**, 117, doi: 10.1029/2011JD017168, 2012.

Griffis, T. J., Wood, J. D., Baker, J. M., Lee, X., Xiao, K., Chen, Z., Welp, L. R., Schultz, N. M., Gorski, G., and Chen, M.: Investigating the source, transport, and isotope composition of water vapor in the planetary boundary layer, **Atmospheric Chemistry and Physics**, 16, 5139-5157, doi: 10.5194/acp-16-5139-2016, 2016.

Kaseke, K. F., Wang, L., Wanke, H., Tian, C., Lanning, M., and Jiao, W.: Precipitation origins and key drivers of precipitation isotope (^{18}O, ^{2}H, and ^{17}O) compositions over windhoek, **Journal of Geophysical Research: Atmospheres**, 123, 7311-7330, doi: 10.1029/2018JD028470, 2018.

Keeling, C. D.: The concentration and isotopic abundances of atmospheric carbon dioxide in rural areas, **Geochimica et Cosmochimica Acta**, 13, 322-334, doi: 10.1016/0016-7037(58)90033-4, 1958.

Keeling, C. D.: The concentration and isotopic abundances of carbon dioxide in rural and marine air, **Geochimica et Cosmochimica Acta**, 24, 277-298, doi: 10.1016/0016-7037(61)90023-0, 1961.

Keppler, F., Schiller, A., Ehehalt, R., Greule, M., Hartmann, J., and Polag, D.: Stable isotope and high precision concentration measurements confirm that all humans produce and exhale methane, **Journal of Breath Research**, 10, 016003, doi: 10.1088/1752-7155/10/1/016003, 2016.

Kerstel, E., and Gianfrani, L.: Advances in laser-based isotope ratio measurements: selected applications, **Applied Physics B**, 92, 439-449, doi: 10.1007/s00340-008-3128-x, 2008.

Kong, Y., Pang, Z., and Froehlich, K.: Quantifying recycled moisture fraction in precipitation of an arid region using deuterium excess, **Tellus B: Chemical and Physical Meteorology**, 65, 19251, doi: 10.3402/tellusb.v65i0.19251, 2013.

Lai, C.T., Ometto, J. P., Berry, J. A., Martinelli, L. A., Domingues, T. F., and Ehleringer, J. R.: Life form-specific variations in leaf water oxygen-18 enrichment in Amazonian vegetation, **Oecologia**, 157, 197-210, doi: 10.1007/s00442-008-1071-5, 2008.

Ma, Q., Zhang, M., Wang, S., Wang, Q., Liu, W., Li, F., and Chen, F.: An investigation of moisture sources and secondary evaporation in Lanzhou, Northwest China, **Environmental Earth Sciences**, 71, 3375-3385, doi: 10.1007/s12665-013-2728-x, 2014.

Mahindawansha, A., Orlowski, N., Kraft, P., Rothfuss, Y., Racela, H., and Breuer, L.:

https://doi.org/10.5194/hess-2020-1
Preprint. Discussion started: 16 January 2020

Quantification of plant water uptake by water stable isotopes in rice paddy systems, **Plant and Soil**, 429, 281-302, doi: 10.1007/s11104-018-3693-7, 2018.

Majoube, M.: Fractionnement en oxygene 18 et en deuterium entre l'eau et sa vapeur, **Journal de Chimie Physique**, 68, 1423-1436, doi: 10.1051/jcp/1971681423, 1971.

Merlivat, L., and Jouzel, J.: Global climatic interpretation of the deuterium-oxygen 18 relationship for precipitation, **Journal of Geophysical Research: Oceans**, 84, 5029-5033, doi: 10.1029/JC084iC08p05029, 1979.

Miller, J. B., and Tans, P. P.: Calculating isotopic fractionation from atmospheric measurements at various scales, **Tellus B**, 55, 207-214, doi: 10.1034/j.1600-0889.2003.00020.x, 2003.

Moreira, M., Sternberg, L., Martinelli, L., Victoria, R., Barbosa, E., Bonates, L., and Nepstad, D.: Contribution of transpiration to forest ambient vapour based on isotopic measurements, **Global Change Biology**, 3, 439-450, doi: 10.1046/j.1365-2486.1997.00082.x, 1997.

Peng, T. R., Liu, K. K., Wang, C. H., and Chuang, K. H.: A water isotope approach to assessing moisture recycling in the island-based precipitation of Taiwan: A case study in the western Pacific, **Water Resources Research**, 47, W08507, doi: 10.1029/2010WR009890, 2011.

Seneviratne, S. I., Lüthi, D., Litschi, M., and Schär, C.: Land–atmosphere coupling and climate change in Europe, **Nature**, 443, 205-209, doi: 10.1038/nature05095, 2006.

Sprenger, M., Herbstritt, B., and Weiler, M.: Established methods and new opportunities for pore water stable isotope analysis, **Hydrological Processes**, 29, 5174-5192, doi: 10.1002/hyp.10643, 2015.

Steen-Larsen, H. C., Sveinbjörnsdottir, A. E., Werner, M., Risi, C., Yoshimura, K., Peters, A., and Rosset, J.: Continuous water vapor isotopic composition observations in the sub-tropical North Atlantic (Bermuda), **EGU General Assembly Conference Abstracts**, 2013.

Stein, A., Draxler, R. R., Rolph, G. D., Stunder, B. J., Cohen, M., and Ngan, F.: NOAA's HYSPLIT atmospheric transport and dispersion modeling system, **Bulletin of the American Meteorological Society**, 96, 2059-2077, doi: 10.1175/BAMS-D-14-00110.1, 2015.

Trenberth, K. E.: Atmospheric moisture recycling: Role of advection and local evaporation, **Journal of Climate**, 12, 1368-1381, doi: 10.1175/15200442(1999)012<1368:AMRROA>2.0.CO;2, 1999.

Unger, S., Máguas, C., Pereira, J. S., Aires, L. M., David, T. S., and Werner, C.: Disentangling drought-induced variation in ecosystem and soil respiration using stable carbon isotopes, **Oecologia**, 163, 1043-1057, doi: 10.1007/s00442-010-1576-6, 2010.

Wang, L., Caylor, K. K., and Dragoni, D.: On the calibration of continuous, high-precision $\delta^{18}O$ and $\delta^{2}H$ measurements using an off-axis integrated cavity output spectrometer, **Rapid Communications in Mass Spectrometry**, 23, 530-536, doi: 10.1002/rcm.3905, 2009.

Wang, L., Caylor, K. K., Villegas, J. C., Barron-Gafford, G. A., Breshears, D. D., and Huxman, T. E.: Partitioning evapotranspiration across gradients of woody plant cover: Assessment of a stable isotope technique, **Geophysical Research Letters**, 37, L09401, doi: 10.1029/2010GL043228, 2010.

Wang, L., Niu, S., Good, S. P., Soderberg, K., McCabe, M. F., Sherry, R. A., Luo, Y., Zhou, X., Xia, J., and Caylor, K. K.: The effect of warming on grassland evapotranspiration partitioning using laser-based isotope monitoring techniques, **Geochimica et Cosmochimica Acta**, 111, 28-38, doi: 10.1016/j.gca.2012.12.047, 2013.

Wei, Z., Yoshimura, K., Okazaki, A., Kim, W., Liu, Z., and Yokoi, M.: Partitioning of evapotranspiration using high-frequency water vapor isotopic measurement over a rice paddy field, **Water Resources Research**, 51, 3716-3729, doi: 10.1002/2014WR016737, 2015.

Yakir, D., and Wang, X.F.: Fluxes of CO_2 and water between terrestrial vegetation and the atmosphere estimated from isotope measurements, **Nature**, 380, 515-517, doi: 10.1038/380515a0, 1996.

Yakir, D., and da SL Sternberg, L.: The use of stable isotopes to study ecosystem gas exchange, **Oecologia**, 123, 297-311, doi: 10.1007/s004420051016, 2000.

Yamanaka, T., and Shimizu, R.: Spatial distribution of deuterium in atmospheric water vapor: Diagnosing sources and the mixing of atmospheric moisture, **Geochimica et Cosmochimica Acta**, 71, 3162-3169, doi: 10.1016/j.gca.2007.04.014, 2007.

Yepez, E. A., Williams, D. G., Scott, R. L., and Lin, G.: Partitioning overstory and understory evapotranspiration in a semiarid savanna woodland from the isotopic composition of water vapor, **Agricultural and Forest Meteorology**, 119, 53-68, doi: 10.1016/S0168-1923(03)00116-3, 2003.

Zhang, Y., Shen, Y., Sun, H., and Gates, J. B.: Evapotranspiration and its partitioning in an irrigated winter wheat field: A combined isotopic and micrometeorologic approach, **Journal of Hydrology**, 408, 203-211, doi: 10.1016/j.jhydrol.2011.07.036, 2011.

Zhao, L., Liu, X., Wang, N., Kong, Y., Song, Y., He, Z., Liu, Q., and Wang, L.: Contribution of recycled moisture to local precipitation in the inland Heihe River Basin, **Agricultural and Forest Meteorology**, 271, 316-335, doi: 10.1016/j.agrformet.2019.03.014, 2019.

https://doi.org/10.5194/hess-2020-1
Preprint. Discussion started: 16 January 2020

Hydrology and Earth System Sciences
Discussions

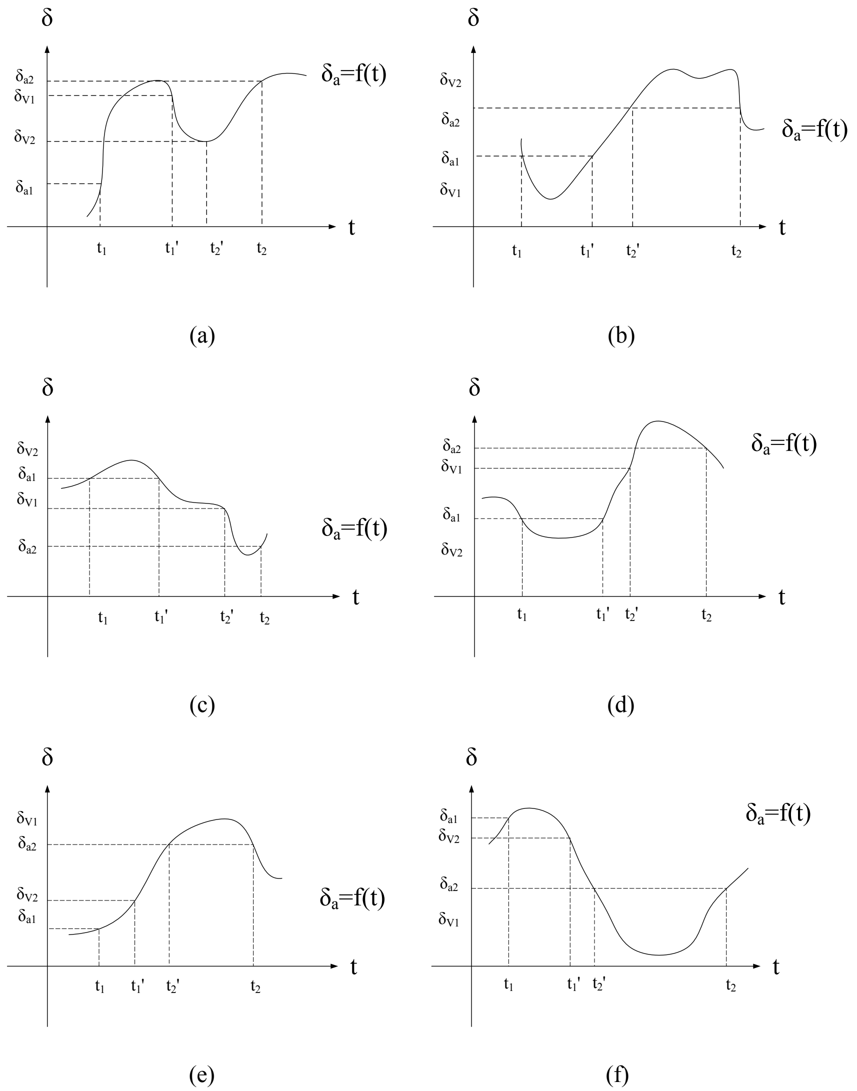

Fig. 1 Theoretical diagrams of all possible combinations of the relationships between isotope composition of ambient vapor (δ_a) and observed isotope composition of atmospheric vapor (δ_v) of two continuous moments t_1 and t_2, ($t_1 < t_2$). δ_{a1} and δ_{a2} represent δ_a value in t_1 and t_2, respectively. δ_{v1} and δ_{v2} represent δ_v value in t_1 and t_2, respectively. t_1' and t_2' represent the time of two specific moments between t_1 and t_2 with $t_1 < t_1' < t_2' < t_2$. For all of the six situations, there exists some sub-intervals $[t_1', t_2'] \subset [t_1, t_2]$ such that the whole range of $\{\delta_a(t): t \in [t_1', t_2']\}$ is within $[min(\delta_{v_1}, \delta_{v_2}), max(\delta_{v_1}, \delta_{v_2})]$.

https://doi.org/10.5194/hess-2020-1
Preprint. Discussion started: 16 January 2020

Hydrology and Earth System Sciences
Discussions

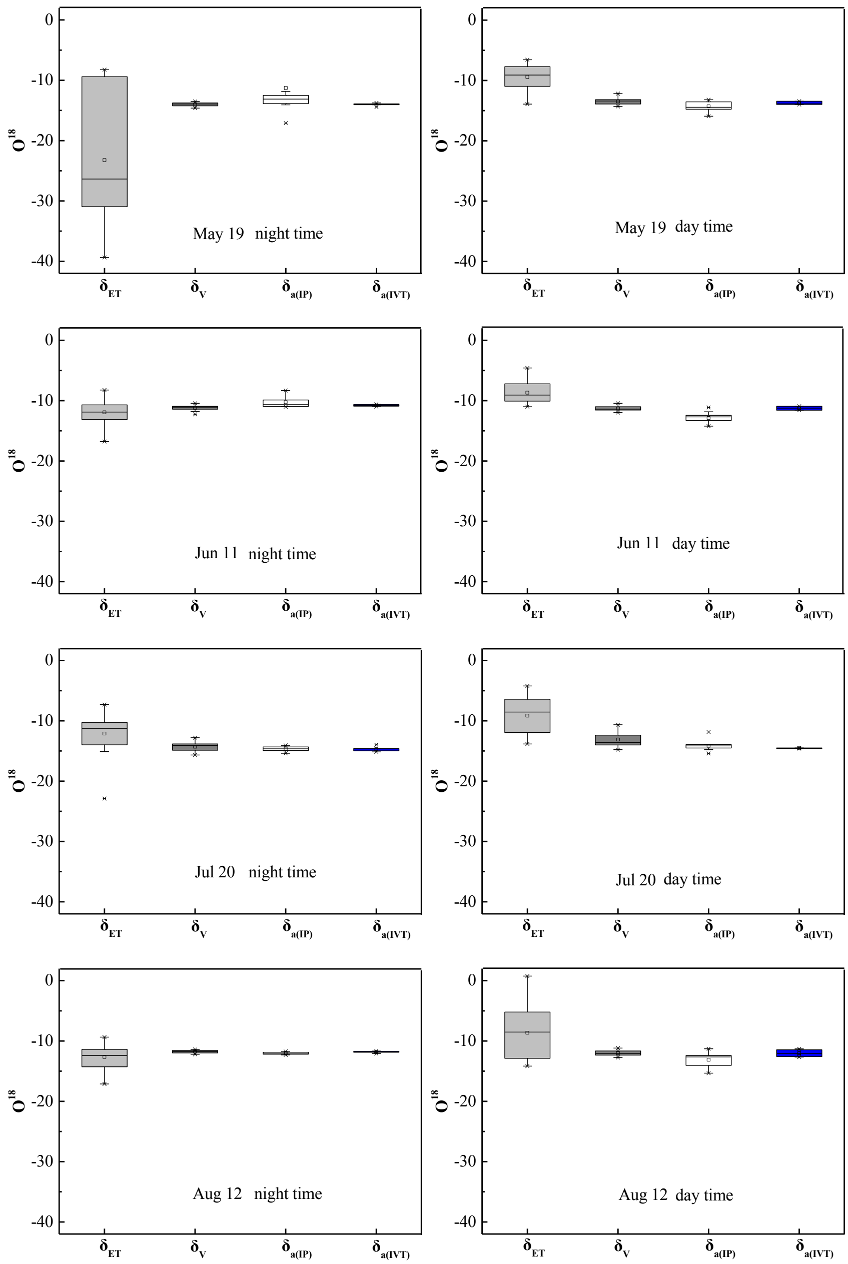

Fig. 2 The average values of the isotope composition of evapotranspiration vapor (δ_{ET}), the isotope composition of atmospheric vapor (δ_v), the estimated isotope composition of ambient vapor using the intersection point method ($\delta_{a(IP)}$) and the Intermediate Value Theorem method ($\delta_{a(IVT)}$) in daytime (7:00 am-7:00 pm) and nighttime (7:00 pm-7:00 am), respectively on May 19th, June 11th, July 20th, and August 12th.

https://doi.org/10.5194/hess-2020-1
Preprint. Discussion started: 16 January 2020

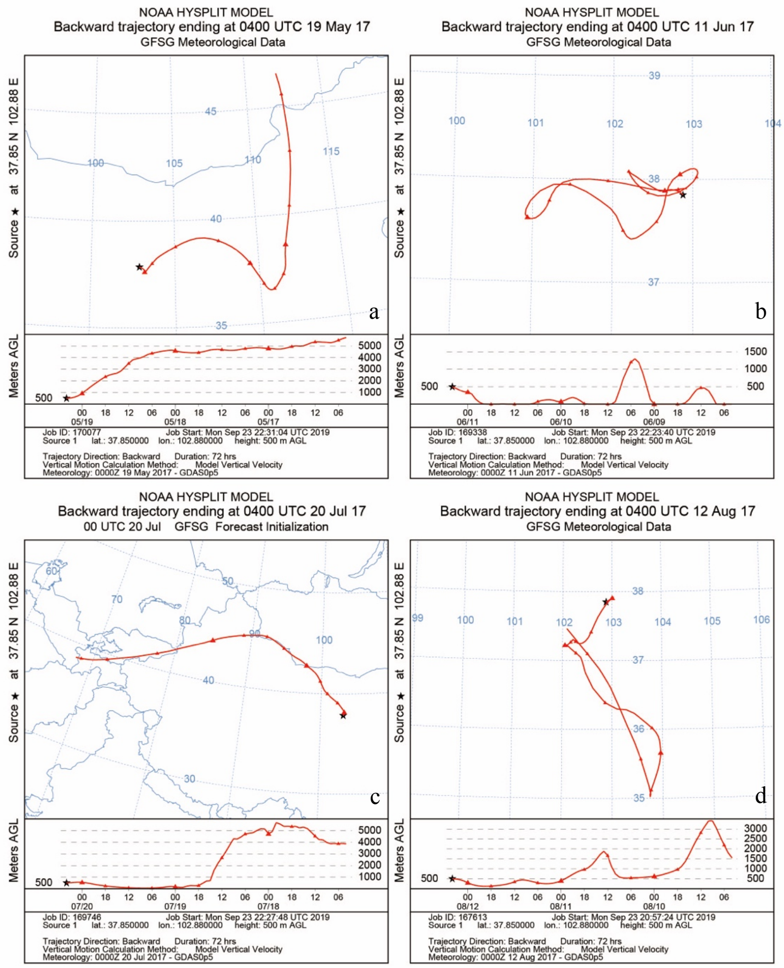

Fig. 3 Hybrid Single Particle Lagrangian Integrated Trajectory (HYSPLIT) backward Trajectory on 19th May (a), 11th June (b), 20th July (c) and 12th August 2019 (d), respectively, which were initialized at 12:00 pm and were calculated backward for 72 hours.

https://doi.org/10.5194/hess-2020-1
Preprint. Discussion started: 16 January 2020

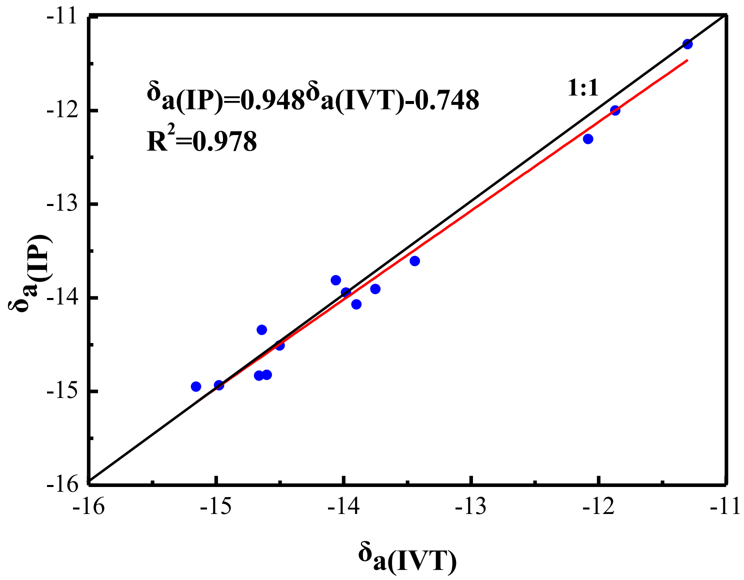

Fig. 4 Linear regression between the estimated isotope composition of ambient vapor using the intersection point method ($\delta_{a(IP)}$) and the Intermediate Value Theorem method ($\delta_{a(IVT)}$) for all the observation periods meeting the criteria of each method.

https://doi.org/10.5194/hess-2020-1
Preprint. Discussion started: 16 January 2020

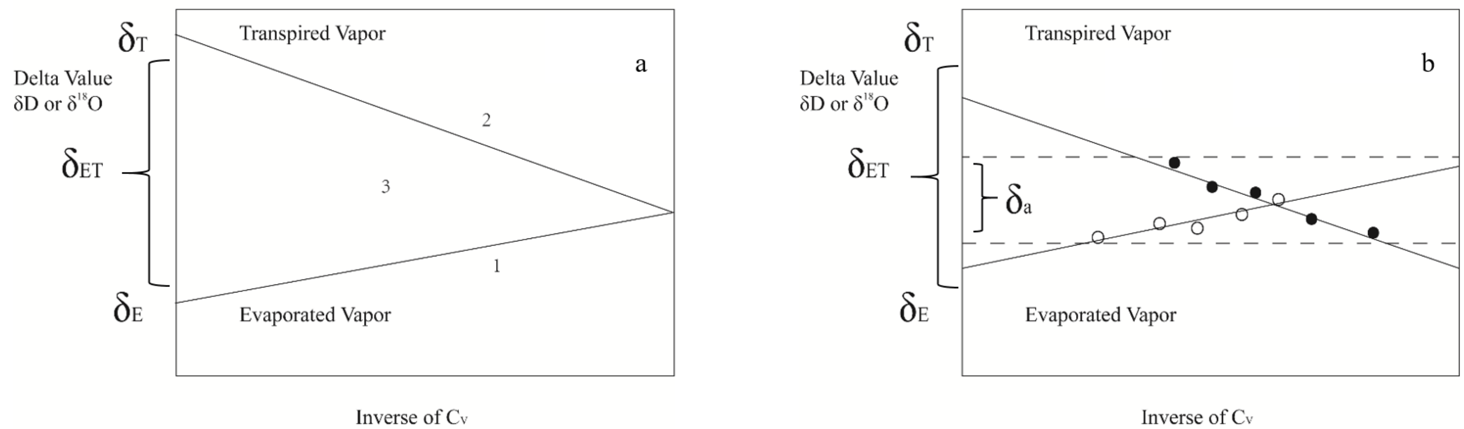

Fig. 5 Hypothetical graph of the idealized Keeling plot curve of the isotope composition of evaporation vapor (δ_E) curve (line 1), the isotope composition of transpiration vapor (δ_T) curve (line 2) and the isotope composition of evapotranspiration vapor (δ_{ET}) curve (area 3) (a), and hypothetical graph of idealized δ_E, δ_T lines and the interval of possible the isotope composition of ambient vapor (δ_a) in the Keeling plots (b).